Comparison of K_I calculation methods

Guian Qian[*1, a], V.F. González-Albuixech[*1, b], Markus Niffenegger[1], Eugenio Giner[2]

1Paul Scherrer Institute, Nuclear Energy and Safety Department, Laboratory for Nuclear Materials, OHSA/06, 5232 Villigen PSI, Switzerland

2 Dpto. de Ingeniería Mecánica y de Materiales, Centro de Investigación en Ingeniería Mecánica – CIIM, Universitat Politècnica de València, Camino de Vera s/n, 46022 Valencia, Spain.

Abstract

This paper compares different numerical methods for mode I stress intensity factor (SIF) calculations. Both 2D and 3D models are used to calculate K_I for the compact tension specimens. *J*-integral and interaction integral provide relatively accurate results. The analysis of a reactor pressure vessel subjected to pressurized thermal shock is performed using the finite element method (FEM) and extended finite element method (XFEM). XFEM method shows advantages in modeling cracks but oscillations in 3D problems due to extraction domains for *J* and interaction integrals. The best results are obtained with domain integrals using a FEM with a refined mesh.

Keywords: stress intensity factor, fracture mechanics, interaction integral, extended finite element method

[*ab] Corresponding author

Tel. +41 56 3102865

Fax. +41 56 3102199

E-mail address: guian.qian@psi.ch

Paul Scherrer Institute

Nuclear Energy and Safety Research Department

Laboratory for Nuclear Materials

OHSA/06

5232 Villigen PSI, Switzerland

Nomenclature

a	crack length, mm
b	plate width, mm
a_i, $b_{i\alpha}$	degrees of freedom for generalized heaviside function and the crack-tip functions
d	a reference distance
ds	length along an arbitrary controur Γ
E	elastic modulus, MPa
E'	E for plane stress, $E/(1-\nu^2)$ for plane strain
error	calculation error
f	point force
$f_{ij}(\theta)$	angular functions of crack-tip stress field
$F_\alpha(\mathbf{x})$	crack-tip functions
G	shear modulus, MPa
h	element size, mm
$h(x,a)$	weight function
$H(x)$	generalized Heaviside function
I	set of all nodes in the mesh
I_n	integration constant
$\mathrm{I}^{(\mathrm{I})}$	interaction integral, MPa·m
J	J-integral, MPa·m
J_a	J-integral using analytical method, MPa·m
k	$3-4\nu$ for plane strain, $(3-\nu)/(1+\nu)$ for plane stress
K	linear elastic stress intensity factor, MPa·m$^{0.5}$
K_I, K_II, K_III	Mode I, II, III linear elastic stress intensity factor, MPa·m$^{0.5}$
K_Iex	exact K_I applied using the boundary conditions
K_IIex	exact K_II applied using the boundary conditions
K_Ic	material fracture toughness, MPa·m$^{0.5}$
n	material hardening coefficient
$N_i(x)$	nodal shape function

P	applied force, N
P_{ij}	Eshelby's tensor
R_q	theoretical height of the elements ring
S_q	theoretical width of the elements ring
r	distance from crack tip, mm
T_i	components of the traction vector
u_y	displacement in y direction, mm
u_i, u_i^L	displacement components and auxiliary displacement components
$V_{(s)}$	a domain which encloses the crack front segment
W	specimen width, mm
x_i	crack tip local coordinates
ν	Poisson's ratio
Γ	integration path around the crack tip
α	weight function
Ω	defined model domain
σ_{ij}, σ_{ij}^L	stress components and auxiliary stress components
σ_{yy}	stress components in y direction
ω	strain energy density, MPa·m$^{-0.5}$
ε	small crack front segment
ε_{ij}, ε_{ij}^L	strain components and auxiliary strain components
u_i	displacement components
θ	angular coordinate in the polar system
δ_{ij}	Kronecker delta
CT	compact tension
DOFs	degrees of freedom
FE	finite element
FEM	finite element method
RPV	reactor pressure vessel
SIF	stress intensity factor

XFEM extended finite element method

1. Introduction

The stress intensity factor (SIF) K proposed by Irwin [1] is the main fracture parameter for the integrity assessment of the structures containing cracks. The SIF quantifies the singularity intensity of an elastic crack-tip stress field, which formed the foundation of linear elastic fracture mechanics, and is used to describe both the crack driving force and the material fracture resistance K_{Ic}. Thus, the SIF K has been widely used in fracture mechanics analysis and structural integrity assessment, e.g. of reactor pressure vessels (RPVs)[2-4]. In such calculations, the question concerning the appropriate method for the calculation of K_I arises. In this paper, we compare and discuss some of the methods used for K_I calculations.

With the fracture parameter K, a simple fracture criterion is expressed as $K \geq K_{Ic}$, where the K depends on applied loads and crack geometry and the K_{Ic} is the fracture toughness of the material measured under conditions in which a plane strain condition prevails. Once K is obtained, elastic crack assessment can be then performed. Thus determination of K is of great engineering significance. It is necessary to calculate K with high accuracy in order to assess the integrity of cracked components precisely.

For simple cracks in specimens and components, analytical and semi-analytical solutions of K have been obtained and are included in different SIF handbooks, such as Murakami et al. [5], Newman and Raju [6] and Al Laham [7]. Based on the weight function concept, some solutions of K have been proposed and included in codes such as ASME Section XI [8], API 579 [9], RSE-M [10] or JSME Code [11]. Most of these proposed solutions take the stress distribution into account as a polynomial equation that extends to the third or fourth order.

However, for an arbitrary crack in complicated structures or under complex loading conditions, there are no closed-form solutions for K. The finite element method (FEM) is usually resorted to calculate K. With the FEM, both the near-tip and full-field solutions of stresses and strains of the complex cracks can be determined. Lots of efforts have been made to use the FEM for calculating K since the 1970s.

The numerical methods for calculating *K* can be divided into the field variable methods and the energy release methods. The field variable methods can be further divided into displacement based and stress based methods. The displacement based methods consist of the displacement extrapolation method proposed by Chan et al. [12]. The quarter-point displacement method by Barsoum [13] and Henshell and Shaw [14], and the displacement correction method by Shih et al. [15] can be used to reproduce the theoretical linear elastic fracture mechanics stress and displacement fields near a crack tip. The stress based methods consist of the stress extrapolation method by Chan et al. [12] and the force method by Raju and Newman [16]. The energy release methods include the *J*-integral method by Rice [17], the stiffness derivative method by Parks [18], the virtual crack extension method by Hellen [19], and the virtual crack closure technique developed by Rybicki and Kanninen [20].

Banks-Sills and Sherman [21] compared the displacement based and energy-based methods, and showed that the *J*-integral and the stiffness derivative method yielded the most accurate results, whereas the displacement extrapolation method was the simplest method with reasonable accuracy. In contrast to the displacement methods, the stress based methods are not often used in the *K* calculations because stresses are calculated from the nodal displacements in a FE simulation and are usually less precise [22]. The energy-based methods generally lead to more accurate *K* through subroutines implemented in the finite element (FE) software. The *J*-integral calculation is available in many commercial FE codes, e.g. ABAQUS [23] and ANSYS [24]. This simplifies the *K* calculation. Zhu [25] showed that the *J*-integral method in the ABAQUS determines accurate *K* values. In addition, ABAQUS adopted an interaction integral method [26] to calculate *K*.

The numerical structural integrity analyses usually rely on the modeling of cracks within the FEM framework. The necessity of a mesh that adapts to the geometry of the component and also to the crack topology imposes some limitations, which entails into simplified models. However, some new techniques have been recently developed that allow the simplification of this kind of analysis. One of these techniques is the extended finite element method (XFEM) which enriches the FE approximation space with special functions that introduce the displacement discontinuity across the crack faces and the singular behavior associated with the crack front, and makes its analysis, up to a certain point, independent of the mesh [28-30]. Furthermore, XFEM has been implemented in the

commercial FE code ABAQUS [23]. It should be noted that due to the XFEM enrichments and the *J*-integral implementation some problems and inaccuracies have been reported [31-32].

This paper aims to compare different numerical methods for K_I calculations. The interaction integral and field decomposition methods using XFEM are briefly analyzed. The displacement extrapolation, the stress extrapolation, the weight function method, the *J*-integral and the interaction integral methods are compared. The simulation is performed for 1T compact tension (CT) specimen, cube specimen containing a curved crack and a RPV model with ABAQUS by means of FE and XFEM methods. Both 2D and 3D models are compared. The main contributions are remarking the well-known applicability of the interaction integral for SIF computation especially for XFEM, and highlighting problems associated with the XFEM method that impose limitations on its accuracy. This study compares models and meshing techniques that correspond to practical examples. The convergence rate of the methods depends on the orientation between the crack and the element borders and the location of the crack within the elements [32, 33]. Thus, the focus of the study is on the applied methods, instead of convergence rate study.

2. Numerical methods for K_I calculation

According to fracture mechanics theory, K_I is a function of the far-field stress, the crack size, the shape and orientation of the crack, and dimensions of the geometry. The following introduces methods in ASTM and those used in FE codes for the calculation of SIF.

2.1 K_I calculated from ASTM geometric factor

According to ASTM [31], K_I for the CT specimen is calculated as

$$K_I = \frac{P}{B\sqrt{W}} \frac{2+\frac{a}{W}}{(1-\frac{a}{W})^{3/2}} \left[0.886 + 4.64\left(\frac{a}{W}\right) - 13.32\left(\frac{a}{W}\right)^2 + 14.72\left(\frac{a}{W}\right)^3 - 5.6\left(\frac{a}{W}\right)^4 \right]. \quad (1)$$

2.2 K_I calculated from displacement distribution

For a Mode I crack, the relationship between the displacement u_y near the crack tip and the SIF is [12]:

$$u_y = \frac{K_I}{2G}\sqrt{\frac{r}{2\pi}}\sin\frac{\theta}{2}[k+1-2\cos^2(\frac{\theta}{2})]. \quad (2)$$

where k=3-4v for plane strain and k=(3- v)/(1+ v) for plane stress.

Thus, SIF at θ=π (i.e. the crack faces) is expressed as

$$K_I = \lim_{r\to 0}\left[\frac{2G}{k+1}\sqrt{\frac{2\pi}{r}}u_y\right]. \quad (3)$$

In a FE calculation, the displacement is calculated and used for SIF calculation in the vicinity of crack tip. The SIF is extrapolated from the displacement values at the crack faces in the vicinity of the crack tip.

2.3 K_I calculated from stress distribution

For a Mode I crack, the relationship between the stress at the crack tip and the SIF at θ=0 is [12]:

$$K_I = \lim_{r\to 0}\left[\sigma_{yy}(r,\theta)\sqrt{2\pi r}\right]. \quad (4)$$

In a FE calculation, the stress is calculated and used for SIF calculation. K_I is extrapolated by the stresses in the vicinity of crack tip.

2.4 K_I calculated from weight function method

According to the weight function concept, if the weight function is known for a crack in a component, the SIF can be obtained by multiplying this function by the stress distribution and integrating it along the crack length [5, 6, 7]. If σ(x) is the normal stress distribution in the uncracked component along the prospective crack line of an edge crack (shown in Fig. 1), the SIF is given by:

$$K_I = \int_0^a \sigma(x)h_I(x,a)dx. \quad (5)$$

The weight function $h(x,a)$ does not depend on the special stress distribution, but only on the geometry of the component. One possibility to derive the weight function is the evaluation of numerically determined crack opening profiles which may be obtained by FE computations. The weight function method simplifies the modeling of the components (no need to model cracked components) and calculates SIF by using analytical equation. However, the precision is sometimes problematic.

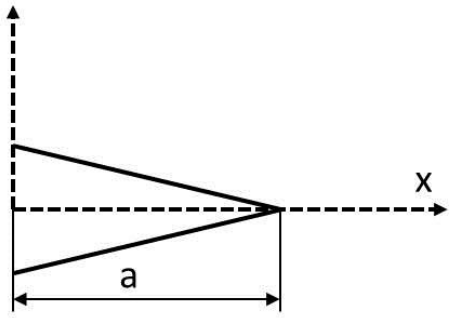

Fig. 1. One-dimensional crack model in weight function method.

2.5 *K* calculated from *J*-integral method

The *J*-integral can be used for the calculation of K_I in linear elastic fracture mechanics. *J*-integral is given as [17]

$$J = \int_{\Gamma} [\omega dx_2 - T_i \partial_1 u_i ds], \tag{6}$$

where ω is the strain energy density, T_i are components of the traction vector, u_i are the displacement vector components and ds is the length along an arbitrary controur Γ. Rice showed that the *J*-integral is path independent.

For linear elastic problems, *J*-integral equals to the energy release rate under a single mode condition. *K* can be calculated from *J*-integral according to the following equation

$$\mathrm{K} = \sqrt{\mathrm{JE}'}, \tag{7}$$

where $E'=E$ for plane stress, and $E'=E/(1-\nu^2)$ for plane strain.

In FEM codes, e.g. ABAQUS and ANSYS, the domain integral method [34] is used to calculate *J*-integral. By using the divergence theorem, *J*-integral in Eq. (6) can be reformulated over a finite domain surrounding the crack tip as follows:

$$J = \int_V \partial_j q_i P_{ij} d\Omega \,, \tag{8}$$

where P_{ij} is the Eshelby's tensor, which is defined as

$$P_{ij} = \frac{1}{2}\varepsilon_{kl}\sigma_{kl}\delta_{ij} - \sigma_{jk}\partial_j u_k \,, \tag{9}$$

where u_i is the displacement field, σ_{ij} is the stress field, δ_{ij} is the Kronecker's delta function and q_i is a vector which is zero on the contour of the extraction domain V and one at the point of the crack front where *J* is evaluated in a 3D problem.

For a structure under proportional loading, good domain independence of *J*-integral is observed in different domains around the crack tip. Because *J*-integral is taken over a domain that usually includes several elements, local errors are minimized.

Note that with *J*-integral, it is not possible to separate the different fracture modes K_I, K_{II} and K_{III}.

2.6 K_I calculated from interaction integral

The interaction integral is used to extract the SIF under mixed mode situations [27], enabling the computation of K_I, K_{II} and K_{III}.. To achieve this goal, auxiliary fields are needed. The interaction integral is derived from the application of the *J*-integral to a problem where two stress fields are involved, resulting in the following decomposition

$$J^{(1+2)} = J^{(1)} + J^{(2)} + I \,. \tag{10}$$

The term *I* corresponds to the interaction integral and includes the interaction between the two intervening fields.

For a straight crack, the interaction integral is written as

$$\mathrm{I} = -\int_{\mathrm{V}} \left(\sigma_{\mathrm{kl}} \varepsilon_{\mathrm{kl}}^{\mathrm{aux}} \delta_{\mathrm{ij}} - \sigma_{\mathrm{kj}}^{\mathrm{aux}} \partial_{\mathrm{i}} \mathrm{u}_{\mathrm{k}} - \sigma_{\mathrm{kj}} \partial_{\mathrm{i}} \mathrm{u}_{\mathrm{k}}^{\mathrm{aux}} \right) \partial_{\mathrm{j}} \mathrm{q}_{\mathrm{i}} \mathrm{d}\Omega \,. \tag{11}$$

The fields denoted with the superscript ^{aux} are the auxiliary fields. Usually, the auxiliary fields are selected to be the straight crack fields, allowing the extraction of the different SIF modes. The fields u_i, σ_{ij}, q_i and the Kronecker's delta δ_{ij} are defined in the same way as in the *J*-integral, being ε_{ij} the strain field. At a point of the 3D crack front, the SIF is

$$\mathrm{K_I} = \frac{\mathrm{E}}{2\left(1-\nu^2\right)} \frac{\mathrm{I}^{(\mathrm{I})}}{\int_{\mathrm{C}} \alpha \mathrm{dc}} . \qquad \text{with} \quad K_{I}^{aux} = 1, \mathrm{K_{II}^{aux}} = \mathrm{K_{III}^{aux}} = 0 \tag{12}$$

$\mathrm{I}^{(\mathrm{I})}$ indicates that the interaction integral is computed using an auxiliary field where only the corresponding mode is nonzero. In our case we only consider the existence of mode I.

The interaction integral method has been implemented in ABAQUS to calculate K_{I}, K_{II} and K_{III}.

2.7 Calculation of the elastic fields by XFEM

XFEM was mainly developed to compute discontinuous and singular problems and also it simplifies the modeling of cracked structures and components. Therefore, XFEM can also be used for calculating SIF. The advantage of XFEM lies in the crack modeling, because no remeshing is needed in the crack growth problems and the crack path can be calculated. Discontinuities can also be within elements. The essential idea of XFEM is to use a displacement field approximation that can model any crack face discontinuity and the near crack-tip asymptotic stress field. As a consequence it is not necessary to modify the mesh to consider a specific crack; at most, moderate refinement must be introduced around the crack to achieve good accuracy. The method is based on the enrichment of the FE description with additional degrees of freedom (DOFs) that are associated with the nodes of the elements affected by the crack [28, 29, 30]. The displacement approximation for the extended finite element formulation used for crack modeling takes the form:

$$\mathbf{u}_{\mathrm{XFEM}}(\mathbf{x}) = \sum_{\mathrm{i}\in\mathrm{I}} \mathrm{N_i}(\mathbf{x})\mathbf{u}_{\mathrm{i}} + \sum_{\mathrm{i}\in\mathrm{J}} \mathrm{N_i}(\mathbf{x})\mathrm{H}(\mathbf{x})\mathbf{a}_{\mathrm{i}} + \sum_{\mathrm{i}\in\mathrm{K}} \left[\mathrm{N_i}(\mathbf{x}) \sum_{\alpha=1}^{4} \mathrm{F}_{\alpha}(\mathbf{x})\mathbf{b}_{\mathrm{i}\alpha} \right], \tag{13}$$

where I is the set of all nodes in the mesh, N_i(x) are the nodal shape function and $\mathbf{u}_i$ are the standard DOFs of node i ($\mathbf{u}_i$ represents the physical nodal displacement for non-enriched nodes only). The subsets J and K contain the nodes enriched with the Generalized Heaviside function H(x) or the crack-tip functions $F_{\alpha}(\mathbf{x})$, respectively, and $\mathbf{a}_i$, $b_{i\alpha}$ are the corresponding DOFs. Fig. 2 shows the enrichment method in XFEM.

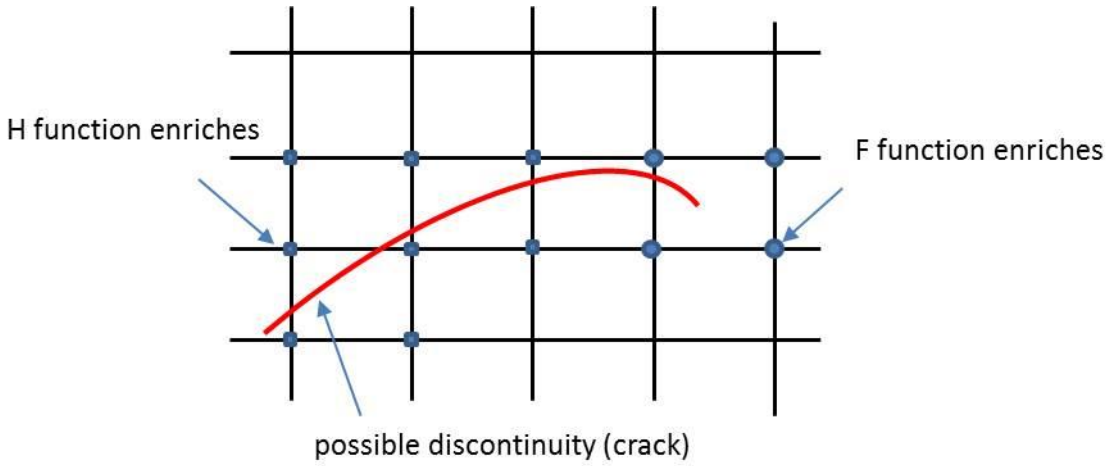

Fig. 2. Enrichment method in XFEM.

The solution of the elastic fields with this method can be used as input for any of the SIF extraction techniques reviewed above, although some techniques such as the domain integral methods are more suitable than others.

3. K_I analysis for CT specimen

3.1 Specimens

The CT specimen has been standardized by the ASTM for use in the experimental determination of the fracture toughness of metallic materials and is used in this study for K_I calculations.

A schematic diagram of a CT test specimen is shown in Fig. 3. Fig. 3(c) shows an example of the mesh and crack details for CT specimen using XFEM. A clevis and pin arrangement is used to hold the specimen. The precracked experimental specimen is modeled allowing the material fracture toughness to be determined in terms of K_I or the J-integral.

3.2 Modeling and mesh

The linear elastic material constitutive properties are defined by the Young's modulus E and Poisson's ratio v. The temperature-independent elastic modulus and Poisson's ratio are assumed to be 200 GPa and 0.3, respectively.

FE simulations are conducted by ABAQUS 6.13. The 1T CT specimens having a thickness *B* of 25 mm with the width *W* of 50 mm and the crack depth *a* to specimen width *W* ratio (*a*/*W*) of 0.5 are modeled. The displacement (0.3mm) is applied on a rigid pin in contact (frictionless) with the specimen and the applied load is obtained from the reaction force acting on the rigid body. 8-node brick elements and 20-node hexahedron elements are used in 2D and 3D models as shown in Fig. 6. Plane strain is assumed in the 2D model. The total number of elements are 2500, 64000 and 70000 for 2D, 3D FE and 3D XFEM models, respectively. Note that the element sizes in these models are about 0.02 mm around the crack front. *J* and K_I are computed based on the domain integral using 20 contours and the interaction integral. In this FE calculation, it is observed that the last several contours give almost path independent values of K_I and *J*-integral.

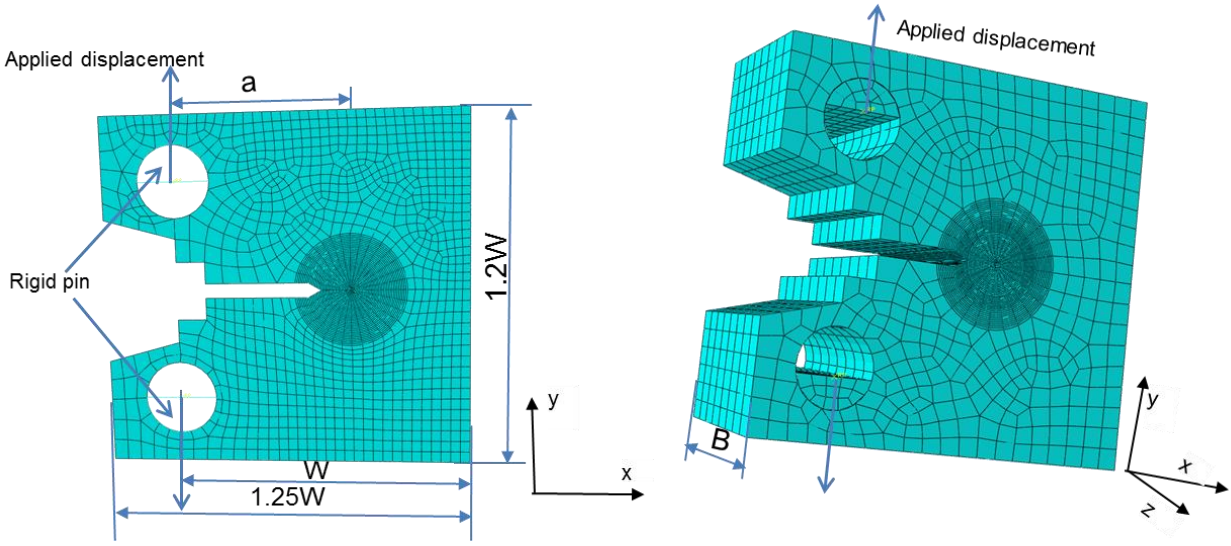

(a) (b)

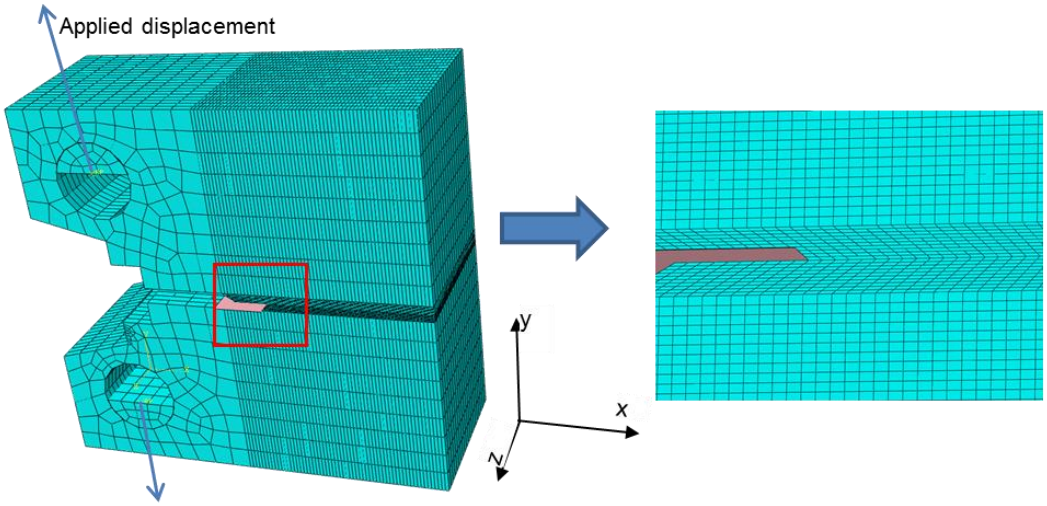

(c)

Fig. 3 Meshes for 2D and 3D CT specimens. (a) Mesh for 2D CT specimen with FEM, (b) mesh for 3D CT specimen for FEM calculation and (c) mesh for 3D CT specimen for XFEM calculation.

3.3 Modelling the crack tip singularity with Abaqus

The stress field around the crack is characterized by a stress singularity at the crack tip [9]. The effect of singularity is proportional to $1/\sqrt{r}$ for elastic materials, where *r* is the distance from the crack front.

In order to simulate the 3D stress singularity for elastic materials with FEM, a 20-node hexahedron (brick) element is used at the crack front but is converted to a wedge element (in ABAQUS it is called C3D20 element). By moving the mid-point nodes to the one-quarter point and keeping the nodes on the cracked face the singularity effect will follow the rule of inverse square root, i.e., $1/\sqrt{r}$ for the crack front, hence avoiding the use of singularity elements in FEM.

3.4. Results

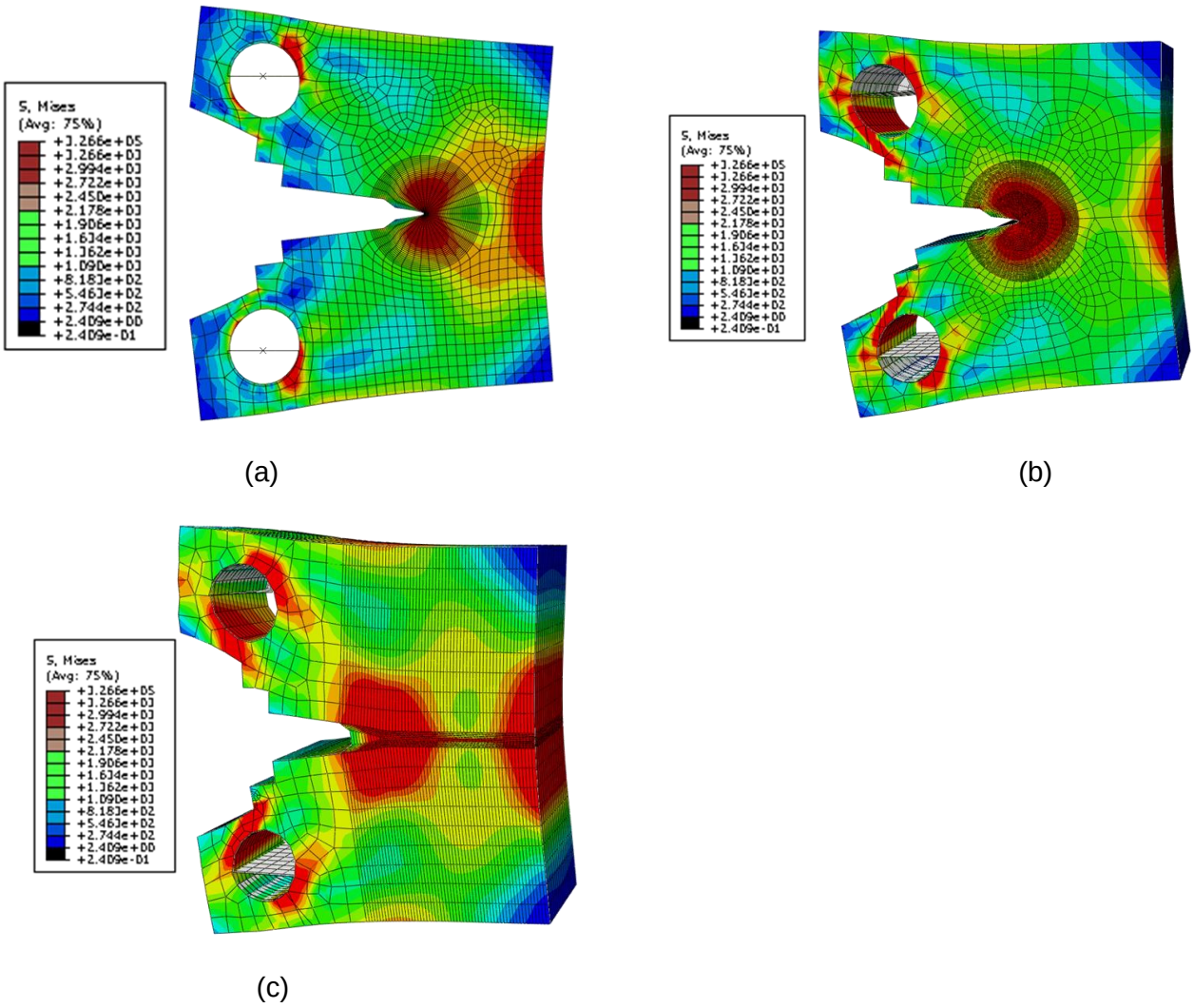

Fig. 4 2D and 3D models for the 1T specimen. (a) 2D model with FE method, (b) 3D model with FEM and (c) 3D model with XFEM method.

The Von Mises stress distributions for the 2D and 3D CT specimens are shown in Fig. 4. A difference of stress distributions in these models can be seen especially at the crack tips, which is due to the mesh discretization. Even so, it is demonstrated in the following that K_I from these models are in general agreement. The reason is that the domain integrals use and integrate results on an extraction region, which overcomes those local errors of stresses and strains. This is an advantage of the domain integral methods in calculating K_I.

By using the displacement extrapolation method, K_I vs. r in the vicinity of the crack tip is computed for the 2D and 3D models and displacement extrapolation results for those models are shown in

Figs. 5 and 6. K_I values are calculated by displacements at different r. Note that the extrapolations for the 3D model are made in the middle layer through the specimen thickness. From Figs. 5 and 6, K_I computed are 3487.4 and 3405.7 MPa mm$^{0.5}$. In a similar way, K_I is calculated using stress extrapolation methods, and the results are shown in Figs. 7 and 8 for 2D and 3D models. From the fitted equations, K_I are 3372.4 and 3269.9 MPa mm$^{0.5}$.

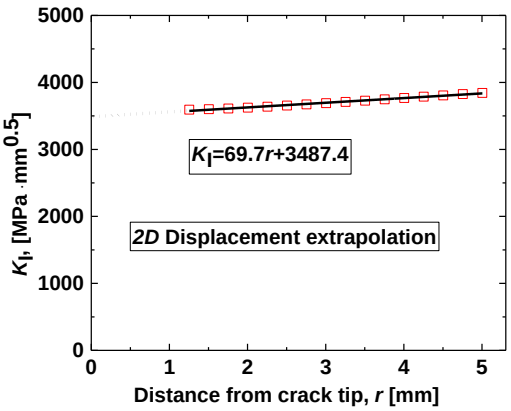

Fig. 5 K_I calculated by displacement extrapolation method with 2D FE model.

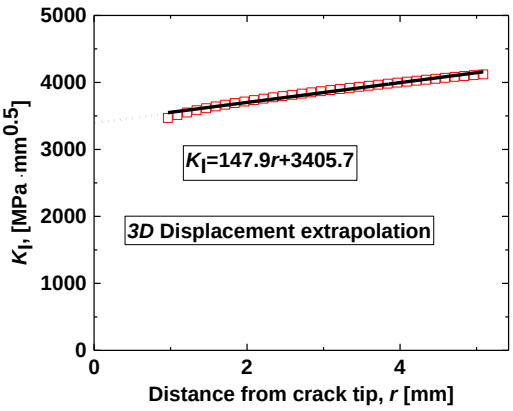

Fig. 6 K_I calculated by displacement extrapolation method with 3D FE model.

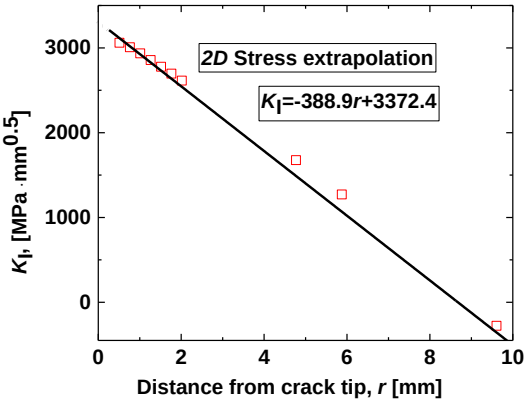

Fig. 7 K_I calculated by stress extrapolation method with 2D FE model.

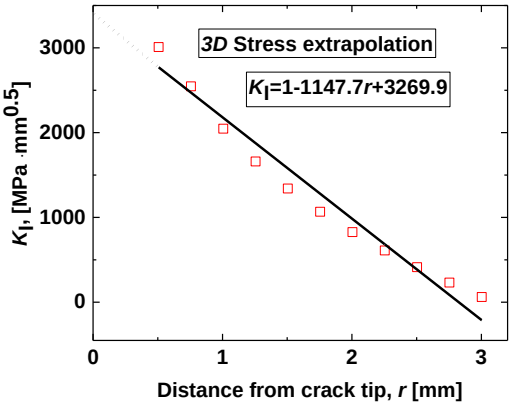

Fig. 8 K_I calculated by stress extrapolation method with 3D FE model.

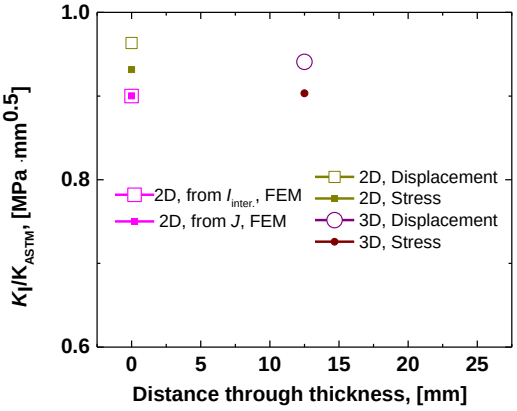

Fig. 9 K_I solution by 2D and 3D models with FE methods.

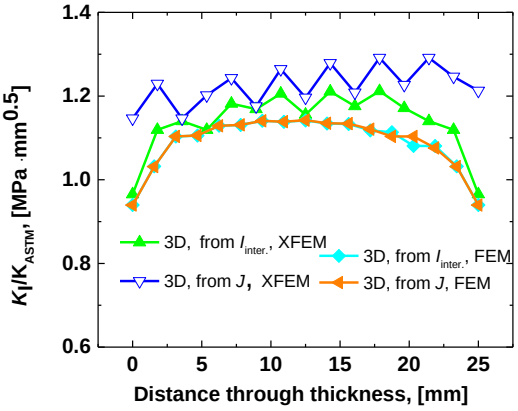

Fig. 10 K_I solution by 2D and 3D models with FE and XFEM methods.

In order to apply the ASTM method for K_I calculation, the applied force P on the specimen should be obtained. By using Eq. (1), K_I is calculated as

$$K_I = \frac{P}{B\sqrt{W}} \frac{2+\frac{a}{W}}{(1-\frac{a}{W})^{3/2}} \left[0.886 + 4.64\left(\frac{a}{W}\right) - 13.32\left(\frac{a}{W}\right)^2 + 14.72\left(\frac{a}{W}\right)^3 - 5.6\left(\frac{a}{W}\right)^4 \right]$$

$$= 3620 \ \text{MPa} \cdot \text{m}^{0.5} \quad . \qquad (14)$$

K_I is also calculated by the J-integral and the interaction integral with 2D and 3D models. Results are compared in Figs. 9 and 10. It is seen that for the 3D models, K_I varies along the thickness direction as the condition varies from higher constraint at the middle of the specimen to lower constraint near the free surfaces. Some oscillations in K_I are observed with the XFEM method. This is due to the limitation of the enrichment function, and limitations with the integral implementation [31-32]. K_I extraction from XFEM shows some differences from one side of the model to the other even on the symmetrical surfaces at different sides. This could be ascribed to derivatives used on the domain integral and to the limitation of the enriching functions. More reasons are still under discussion for the XFEM community. This behavior has been reported in different programs and with slightly different domain integral implementations. It constitutes the improvement of the domain integral implementation for avoiding or minimizing the oscillations. Therefore, the proper application of XFEM in fracture mechanics is a future research topic. The results from

displacement and stress distribution methods are lower than those from interaction and *J*-integral. 2D model results in a lower K_I. Through the 3D model thickness, constraint loss occurs and thus plane strain condition does not hold along the crack front. We compare both the *J* and interaction integrals for K_I calculation.

It shall be noted that since in this study the meshes are relatively fine (average size 1.5 mm), a mesh sensitivity study is not performed.

4. K_I (*J*) analysis for curved crack in a cube

In this Section, *J*-integral is computed with XFEM and FEM for a penny shaped crack in a cube. The comparison is performed using the analytical solution for this problem (e.g. [5]). For the penny shaped crack under remote loading in an infinite body, analytical solution of K_I for this type of crack is

$$\mathrm{K_I} = 2\sigma\sqrt{\frac{\mathrm{a}}{\pi}}\,. \tag{15}$$

The cube model has a width of 2*b*, length of 2*b* and height of *b*. The crack is located at the center of the cube and its radius is defined as *b*/5. The ratio between crack and body geometry allows the acceptance of the infinite domain assumption behavior. The analytical K_I is converted to *J*-integral using Eq. (7). Note that the goal of the study is to show the oscillation of J-integral. The ratio of crack radius to cube half width is assumed not to be critical for the study.

The meshes used in this Section are shown in Fig. 11. The XFEM model uses only symmetries in the x and y plane. The ABAQUS routine fails the crack definition if the symmetry plane lies on the crack plane. Thus the z-plane (crack plane) symmetry is not used. The XFEM mesh, as shown in Fig. 11 (a), is built with a regular linear hexahedrons 3D grid, with the element size of *b*/40. A mesh adapted to the crack geometry can be used to minimize the calculation error in the XFEM study. Fig. 11 (b) shows the mesh, adapted to the crack geometry and with the element size of *b*/200 at crack front. The FE model takes advantage of the symmetries in planes x, y and z, and consequently only one-eighth is considered, as shown in Fig. 11 (c). The FE mesh uses quadratic hexahedron and wedge elements. The elements along the crack front are quadratic wedge with a

size of *b*/200. The ring surrounding the crack is defined by a radius of *b*/10, and the approximate element size is *h*=*b*/100. 10 element rings are available for the domain integral computation.

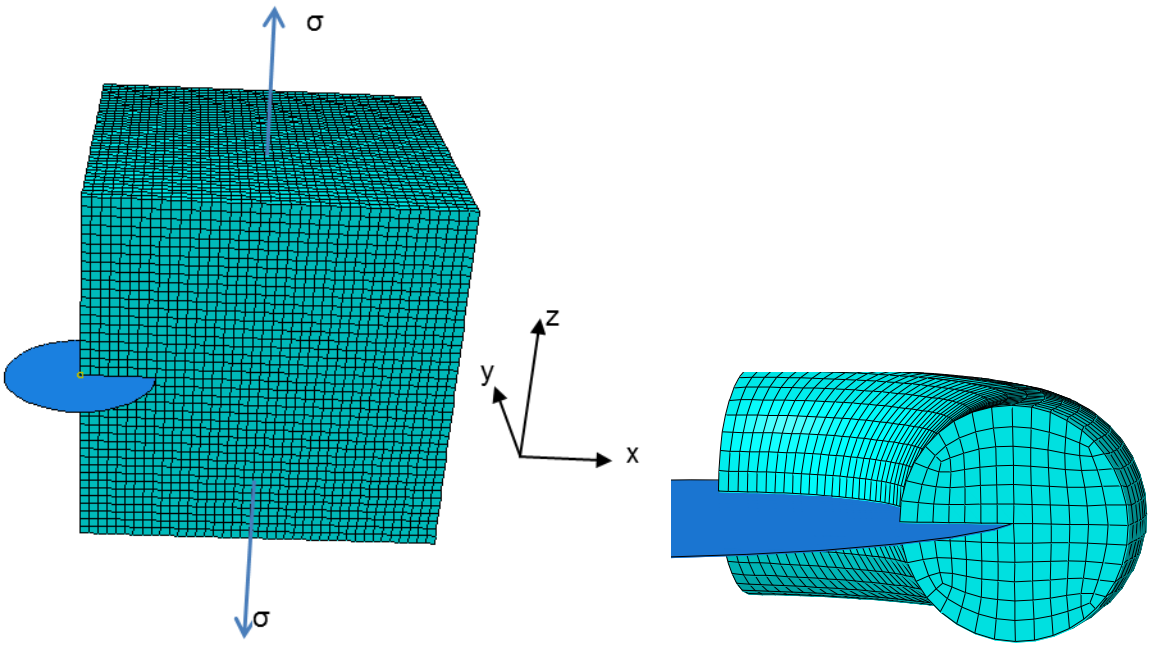

(a) (b)

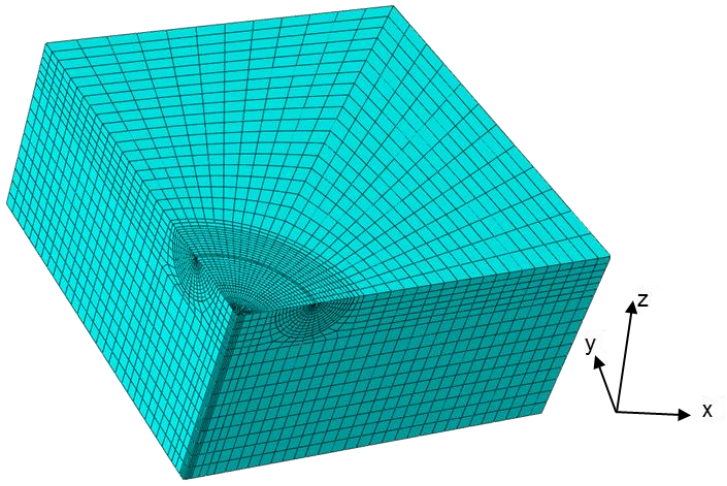

(c)

Fig. 11 Meshes for cube specimen with curved crack (a) Mesh with XFEM method with hexahedron elements, (b) Mesh with XFEM with adapted mesh, (c) Mesh with FEM.

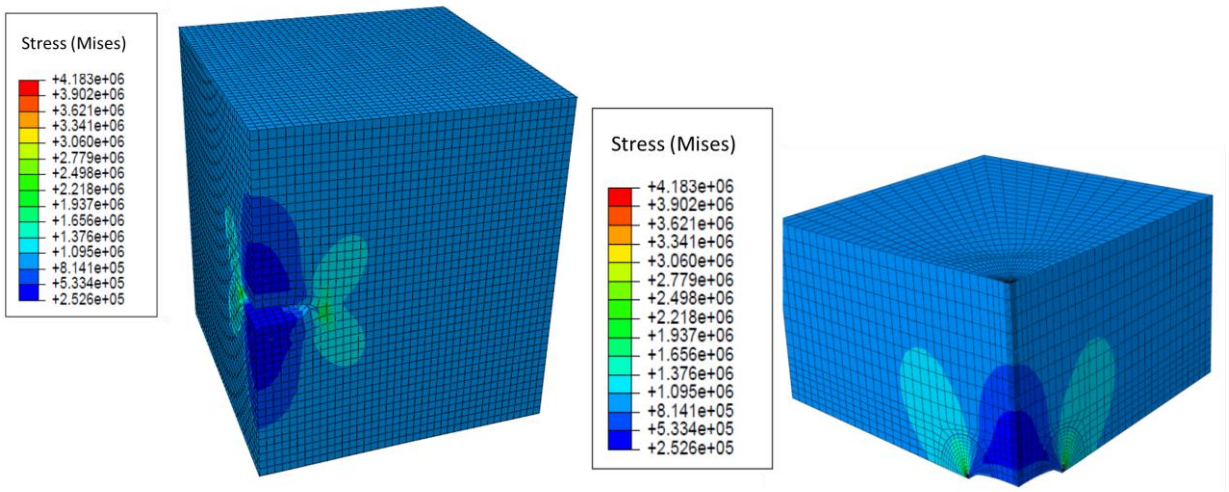

(a) (b)

Fig. 12 Stress distributions and deformation for the cube specimen containing a curved crack (a) Model with XFEM model, (b) Model with FEM method.

Fig. 12 shows the stress distribution and deformation shapes for the XFEM and FEM models. Difference of stress distributions between these two models exists. This is due to the mesh discretization, as described in Section 3.4.

J-integral results along the crack front for the first 8 contours are shown in Fig. 13. *J* is calculated with XFEM and FEM and J_a is calculated analytically with Eqs. (15) and (7). It is seen that there is some oscillations with XFEM and in Fig. 13 (b) that an improvement in the *J* results can be observed with the adapted mesh in XFEM and also the oscillations almost disappear at crack points away from the border. However, the decrease of *J* when approaching to the boundary is not what is expected, because these boundaries are symmetrical, which should lead to non-decreasing values. This may be due to the implementation of XFEM in ABAQUS. In comparison, it is shown in Fig. 13 (c) that with FEM, the last 7 contours result in the best convergence of *J*-integrals. *J*-integral is considered in this comparison as it corresponds to a pure mode situation.

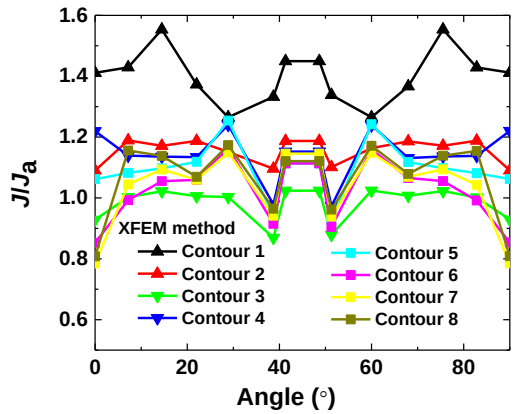

(a)

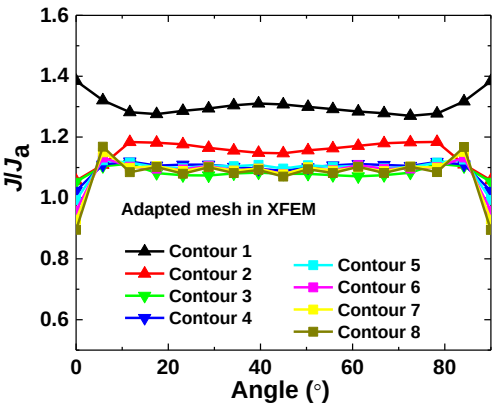

(b)

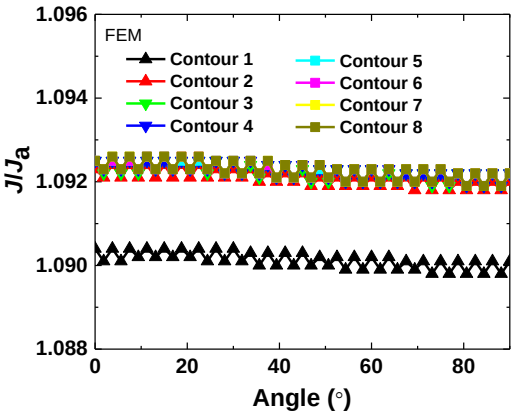

(c)

Fig. 13 *J*-integral along the curved crack front (a) Results with XFEM method with hexahedron elements, (b) Results with XFEM with adapted mesh, (c) Results with FEM.

Oscillation with XFEM can be ascribed to the effect of the relative topology between crack and mesh. This difference affects the definition of the contour ring, which varies from one location to another. Hence, the effective extraction domain shows oscillations as it is associated with the crack location. This effect can be observed in Fig. 14, where S_q and R_q define the theoretical width and height of the elements ring for each point of computation (P), whereas the actual extraction domains for the integral are shaded.

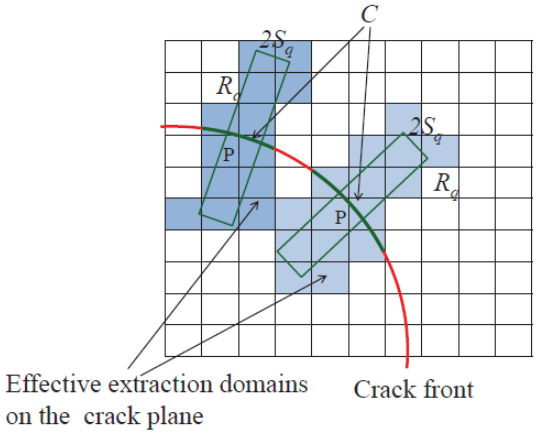

Fig. 14 Effective extraction domain definition.

Fig. 15 compares the results of XFEM and FEM for the last contour ring (8th ring). In agreement with Fig. 13, it is shown that the XFEM case with a mesh non adapted to the crack geometry exhibits oscillations. Note that this is a comparison with very coarse mesh for XFEM and it's not intended for industrial use. The results for the XFEM case with adapted mesh are comparable to the FE mesh, except at the surface border. The best results, as expected, correspond to the refined mesh in the FE approach.

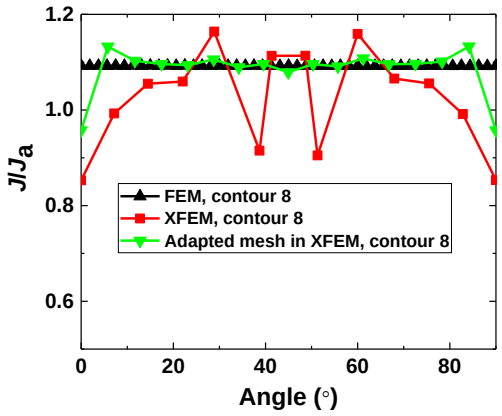

Fig. 15 J/J_a for FEM, XFEM and XFEM with adapted mesh at the contour 8.

From the above study, it is shown that the undesirable oscillation effect with XFEM can be minimized if a crack adapted mesh is used. It is also possible to compute the domain integrals using tetrahedron elements, which may improve the versatility of the XFEM method for complicated structures [33]. However, the analyst should be warned about strong oscillations that may appear in the results (this issue is not commented in the ABAQUS documentation).

5. K_I analysis for a cracked reactor pressure vessel

In this study, a RPV containing a crack is assumed to be subjected to pressurized thermal shocks initiated by a postulated medium loss-of-coolant transient. The history of the water temperatures, pressures and heat transfer coefficients between water and inner wall of the RPV for the transient are those in [4, 35]. The RPV has a radius of 1668.5 mm and thickness of 171 mm. A semi-elliptical surface crack with axial orientation is postulated in the RPV. The depth of the crack is 17 mm and the length is 102 mm. Thermal and structural analyses are performed for the whole transient. The thermal and stress analyses are treated as an uncoupled problem, meaning that the temperature field is firstly calculated, and stresses and strains are computed based on the thermal analysis. The thermo-mechanical properties of the base material and cladding at different temperatures are listed in Tab. 1. The mean coefficient of linear thermal expansion is used and the reference temperature, from which the total thermal expansion is defined, is 20 °C.

Tab. 1. Thermo-mechanical properties of the base material and cladding of the RPV.

	Base material						Cladding					
Temperature [°C]	0	20	100	200	300	400	0	20	100	200	300	400
Elastic modulus [10^3 MPa]	206	206	199	190	181	172	200	200	194	186	179	172
Mean linear thermal expansion coefficient [10^{-6} °C^{-1}] T_{ref}=20 °C	10.3	10.3	11.1	12.1	12.9	13.5	16	16	16	17	17	18
Thermal conductivity [W/(m·K)]	44.4	44.4	44.4	43.2	41.8	39.4	15	15	16	17	19	21
Specific heat capacity [J/(kg·K)]	450	450	490	520	560	610	500	500	500	540	540	590
Density [10^3 kg/m^3]	7.6	7.6	7.6	7.6	7.6	7.6	7.6	7.6	7.6	7.6	7.6	7.6
Poisson's ratio	0.3	0.3	0.3	0.3	0.3	0.3	0.3	0.3	0.3	0.3	0.3	0.3
Yield stress of the unirradiated material [MPa]		449										
Stress free temperature [°C]	280.3											

By taking advantage of symmetry (boundary condition for structural mechanics analysis), one quarter of the RPV is modeled for the FEM calculation, as shown in Fig. 16. The temperature distribution through the vessel wall is obtained in the thermal analysis and is used for fracture mechanics analysis.

The quadratic 20-node hexahedron (brick) element is used for the FE simulation. In order to

simulate the stress singularity for elastic materials, the brick element is converted to a wedge element (it is called C3D20 element in ABAQUS). By moving the mid-point nodes to the one-quarter point and keeping the nodes on the cracked face, the singularity effect will follow the rule of inverse square root, i.e., $1/\sqrt{r}$ for the crack front, as shown in Fig. 16. Mesh details for XFEM analysis is shown in Fig. 17. The XFEM mesh only uses linear hexahedrons, and is coarser that the FEM mesh. Furthermore, the XFEM mesh is only refined where the SIF is intended to be computed.

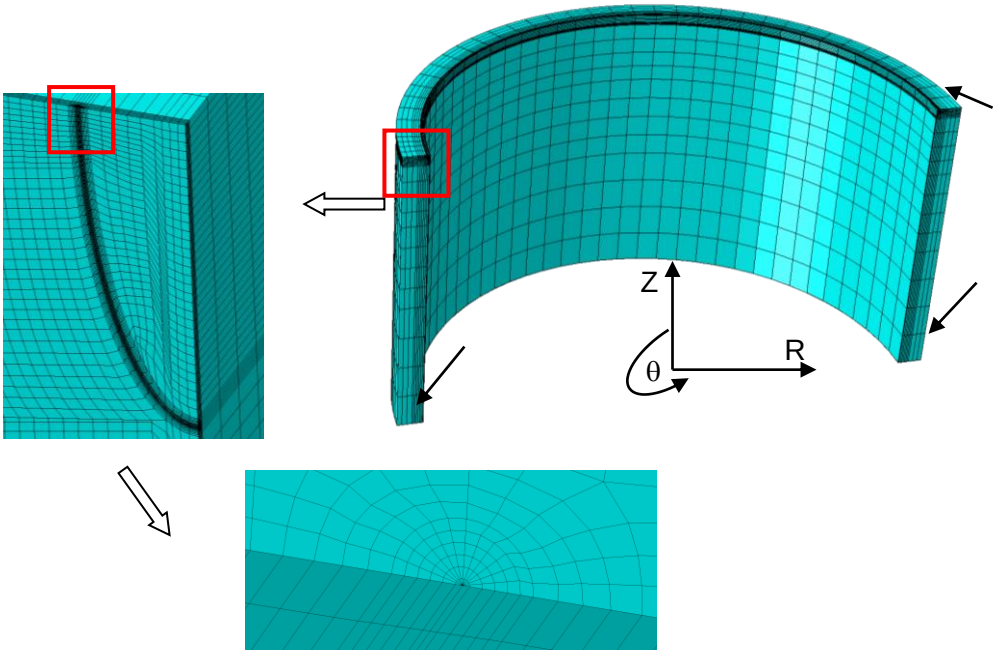

Fig. 16. 3-D model of the beltline region of the RPV for FEM analysis. Due to the symmetry conditions, only one quarter of the model is considered. The $R\theta$ plane, RZ planes indicated with arrows are symmetrical planes.

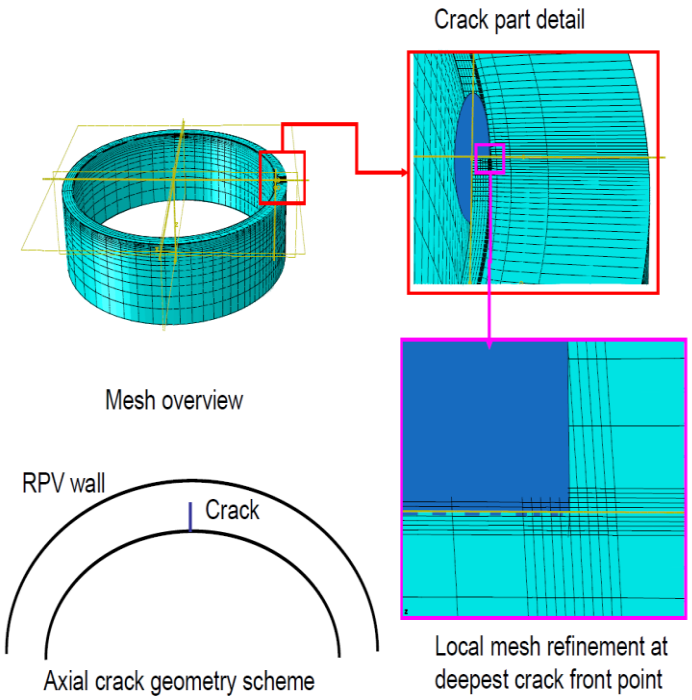

Fig. 17. Mesh details for XFEM analysis.

Fig. 18 shows the mode I SIF vs. crack tip temperature (thermal shock history) for the whole transient. The SIFs calculated from FEM, weight function method and XFEM (by the interaction integral method, as it is not a pure mode I problem) are compared for the crack deepest point, where the maximum SIF is expected. Note that with weight function method, SIF is calculated based on 2D model. The results are quite similar for all cases, showing the good XFEM performance. Some differences may be due to the domain integral implementation of XFEM. However, the agreement between results from all the three methods at the position with maximal K_I is rather good. Also the discrepancy seems to be acceptable in view of the additional uncertainties in the calculations which may lie in the transient itself, in the heat transfer coefficients and temperature distribution.

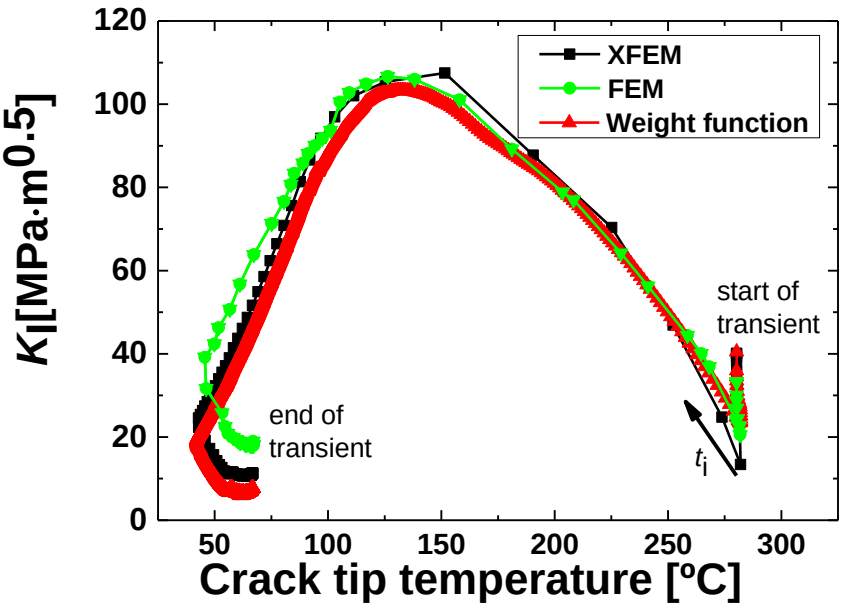

Fig. 18. Comparison of SIF calculated with conventional FEM and XFEM for an axial crack.

6. Conclusions

In this paper, five selected methods (displacement distribution, stress distribution, weight function method, *J*-integral, interaction integral) are applied to calculate and compare K_I values by using the FE software ABAQUS. The selected methods are compared using the compact tension specimen. Results from FEM and XFEM calculations of a cube containing a curved crack and pressurized thermal shock load on a RPV are also compared. From the results, it can be concluded that:

(1) The *J*-integral method and the interaction integral given by ABAQUS provide consistent *K* values with the one calculated by ASTM. Thus, they are appropriate methods to determine accurate *K* values for both 2D and 3D cracks.

(2) The displacement and stress extrapolation method provide consistent results with reasonable accuracy. Both methods can be used for a SIF calculation once the stress and displacement distributions are available. K_I values are lower than those with *J*-integral or interaction integral and similar to the surface values (lower constraint).

(3) 3D model provides more accurate results than 2D models. The difference of stress distributions in 2D, 3D models using FEM and XFEM is due to the mesh discretization. However, K_I from these

methods are in general agreement.

(4) XFEM shows advantages in modeling crack and provides reasonable results. The K_I values along the crack front showed oscillations, which may be due to the limitation of the enrichment function, and limitations of the energy release integral implementation and the extraction domains. The oscillations can be decreased by using the adapted mesh at the crack tip. XFEM is recommended in modeling complicated cracks and structures. However, care should be given to the oscillation of the results.

(5) With *J*-integral, it is not possible to separate K_I, K_{II} and K_{III}. However, this disadvantage can be solved by using the interaction integral method. The interaction integral is the most consistent method.

It is concluded that K_I from different methods applied to the considered models are in general agreement. The better results are obtained from the domain integrals. The reason is that the integrating over a domain minimizes and overcomes the local errors of stresses and strains, since the FEM is based on weak forms and behaves better over domains. This is an advantage of the domain integral methods in calculating K_I.

XFEM has demonstrated its advantage in modeling multiple complicated cracks, e.g. the quasi-laminar indications detected at Doel 3 and Tihange 2 nuclear power plants during the 2012 outage [36, 37]. The observed indications could be attributed to hydrogen flaking induced during the vessel manufacturing process. These kinds of flaws have not yet been documented in ASME code and not were analyzed before. We performed Integrity assessment of a RPV containing multiple laminar flaws using XFEM, as referred in [38]. However, there are still some discussions with XFEM, especially for curved and non planar cracks, which makes its applications only recommended when no other method is feasible.

Acknowledgements

The authors are grateful for the financial support of the PISA Project provided by the Swiss Federal Nuclear Safety Inspectorate (ENSI) (DIS-Vertrag Nr. H-100668). Guian Qian is also grateful for the visiting invitation provided by Key Laboratory of Pressurized Systems and Safety (East China University of Science and Technology), Ministry of Education, China.

7. References

1. Irwin GR. Analysis of Stresses and Strains near the End of A Crack Traversing A Plate. Journal of Applied Mechanics 1957; 24: 361-64.
2. Qian G, Niffenegger M. Investigation of constraint and warm prestressing effects by means of a local approach to fracture. Engineering Fracture Mechanics 2015; 136: 26-37.
3. Qian G, Gonzalez-Albuixech VF, Niffenegger M. In-plane and out-of-plane constraint effects under pressurized thermal shocks. International Journal of Solids and Structures 2014; 51: 1311-1321.
4. Qian G, Niffenegger M. Integrity analysis of a reactor pressure vessel subjected to pressurized thermal shocks by considering constraint effect. Engineering Fracture Mechanics 2013; 112-113: 14-25.
5. Murakami Y. Stress Intensity Factors Handbook. Pergamon Press, 1987.
6. Newman JC, Raju IS. Stress-Intensity Factor Equations for Cracks in Three-Dimensional Finite Bodies Subjected to Tension and Bending Loads, NASA Technical Memorandum 85793, Langley Research Center, 1984.
7. Al Laham S. Stress Intensity Factor and Limit Load Handbook, British Energy Generation Ltd, 1999.
8. ASME, ASME B&PV Code Section XI, Rules for Inservice Inspection of Nuclear Power Plant Components, American Society of Mechanical Engineers, New York, 2013.
9. API/ASME, Recommended Practice for Fitness-for-Service, American Petroleum Institute and the American Society of Mechanical Engineers, API 579-1/ASME FFS-1, 2007.
10. Marie S, Chapuliot S, Kayser Y, Lacire MH, et al. French RSE-M and RCC-MR Code Appendices for Flaw Analysis: Presentation of the Fracture Parameters Calculation – Part III: Cracked Pipes. International Journal of Pressure Vessels and Piping 2007; 84: 614-658.
11. JSME, Rules on Fitness-for-Service for Nuclear Power Plants, The Japan Society of Mechanical Engineers, JSME S NA1-2012, Tokyo, 2012.
12. Chan SK, Tuba LS, Wilson WK. On the Finite Element Method in Linear Fracture Mechanics. Engineering Fracture Mechanics 1970; 2: 1-17.

13. Barsoum RS. Application of Quadratic Isoparametric Finite Elements in Linear Fracture Mechanics. International Journal of Fracture 1974; 10: 603-605.
14. Henshell RD, Shaw KG. Crack Tip Finite Elements Are Unnecessary. International Journal for Numerical Methods in Engineering 1975; 9: 495-507.
15. Shih CF, deLorenzi HG, German MD. Crack Extension Modeling with Singular Quadratic Isoparametric Element. International Journal of Fracture 1976; 12: 647-651.
16. Raju IS, Newman JC. Three-Dimensional Finite Element Analysis of Finite-Thickness Fracture Specimens. NASA TN D-8414, 1977.
17. Rice JR. A Path Independent Integral and the Approximate Analysis of Strain Concentrations by Notches and Cracks. Journal of Applied Mechanics 1968; 35: 379-386.
18. Parks DM. A Stiffness Derivative Finite Element Technique for Determination of Crack Tip Stress Intensity Factors. International Journal of Fracture 1974; 10: 487-502.
19. Hellen TK. On the Method of Virtual Crack Extension. International Journal for Numerical Methods in Engineering 1975; 9: 187-207.
20. Rybicki EF, Kanninen MF. A Finite Element Calculation of Stress Intensity Factors by a Modified Crack Closure Integral. Engineering Fracture Mechanics 1977; 9: 931-938.
21. Banks-Sills L, Sherman D. Comparison of Methods for Calculating Stress Intensity Factors with Quarter-Point Elements. International Journal of Fracture 1986; 32: 127-140.
22. Lim LL, Johnson LW and Choi SK. Comparison between Various Displacement-based Stress Intensity Factor Computation Techniques. International Journal of Fracture 1992; 58: 193-210.
23. ABAQUS/Standard Version 6.12-2, Analysis User's Manual, Dassault Systémes Simulia Corporation, Providence, RI, 2013.Hibbitt, Karlsson, Sorensen, 2012. Abaqus 6.12.3 Manual.
24. ANSYS User's Manual Revision 12.1, ANSYS Inc., Canonsburg, PA, 2012.
25. Zhu XK. Numerical Determination of Stress Intensity Factors Using ABAQUS. Proceedings of the ASME 2014 Pressure Vessels & Piping Conference, PVP2014-28981.
26. Shih CF, Asaro RJ. Elastic-Plastic Analysis of Cracks on Bimaterial Interfaces: Part I-Small Scale Yielding. Journal of Applied Mechanics 1988; 55: 299-316.
27. Moran B, Shih CF. Crack tip and associated domain integrals from momentum and energy balance. Engineering Fracture Mechanics 1987; 27: 615–642.

28. Moës N, Dolbow J, Belytschko T. A finite element method for crack growth without remeshing. International Journal for Numerical Methods in Engineering 1999; 46: 131–150.
29. Moës N, Gravouil A, Belytschko T. Non-planar 3D crack growth by the extended finite element and level sets —Part I: Mechanical model. International Journal for Numerical Methods in Engineering 2002; 53: 2549–68.
30. Sukumar N, Moës N, Moran N, Belytschko T. Extended finite element method for three-dimensional crack modelling. International Journal for Numerical Methods in Engineering 2000; 48: 1549–70.
31. González-Albuixech VF, Giner E, Tarancón JE, Fuenmayor FJ, Gravouil A. Convergence of domain integrals for stress intensity factor extraction in 2-D curved cracks problems with the extended finite element method. International Journal for Numerical Methods in Engineering 2013; 94: 740–757.
32. González-Albuixech VF, Giner E, Tarancón JE, Fuenmayor FJ, Gravouil A. Domain integral formulation for 3-D curved and non-planar cracks with the extended finite element method. Computer Methods in Applied Mechanics and Engineering 2013; 264: 129-144.
33. González Albuixech VF. Estudio de las singularidades de frente de grieta y de esquina en grietas tridimensionales mediante el método de los elementos finitos extendido. Universitat Politècnica de València. doi:10.4995/Thesis/10251/19116, 2012.
34. Li FZ, Shih CF, Needleman A. A comparison of methods for calculating energy release rates, Engineering Fracture Mechanics 1985; 21:405-421.
35. González-Albuixech VF, Qian G, Niffenegger M. Integrity analysis of reactor pressure vessels subjected to pressurized thermal shocks by XFEM. Nuclear Engineering Design 2014; 275: 336-343.
36. Safety case report: Doel 3 – Reactor Pressure Vessel Assessment ; Electrabel, 5/12/2012.
37. Safety case report: Tihange 2 – Reactor Pressure Vessel Assessment ; Electrabel, 5/12/2012.
38. González-Albuixech VF, Qian G, Niffenegger M. XFEM integrity analysis of quasi laminar flaws in a reactor pressure vessel subjected to pressurized thermal shocks. Nuclear Engineering and Design, 2014 (280) 464-72.

Highlights:

The accuracy of different numerical methods of SIF calculation is compared

XFEM method shows advantages in modeling crack

XFEM shows oscillations due to extraction domains for J and interaction integrals

The best results are with domain integrals using a FEM solution with a refined mesh